

PREPARED FOR SUBMISSION TO JCAP

DEMNUi: the Sunyaev-Zel'dovich effect in the presence of massive neutrinos and dynamical dark energy

**Davide Luchina,^{a,b} Mauro Roncarelli,^c Matteo Calabrese,^{d,b}
Giulio Fabbian^e and Carmelita Carbone^b**

^aDipartimento di Fisica “Aldo Pontremoli”, Università degli Studi di Milano, via Celoria 16, I-20133 Milano, Italy

^bINAF – Istituto di Astrofisica Spaziale e Fisica cosmica di Milano (IASF-MI), via Alfonso Corti 12, I-20133 Milano, Italy

^cINAF – Osservatorio di Astrofisica e Scienza dello Spazio di Bologna (OAS-BO), via Piero Gobetti 93/3, I-40129 Bologna, Italy

^dAstronomical Observatory of the Autonomous Region of the Aosta Valley (OAVdA), Loc. Lignan 39, I-11020, Nus (Aosta Valley), Italy

^eSchool of Physics and Astronomy, Queen’s Buildings North Building, 5 The Parade, Newport Road, Cardiff, CF24 3AA, United Kingdom

E-mail: davide.luchina@studenti.unimi.it, mauro.roncarelli@inaf.it, calabrese@oavda.it, fabbian@cardiff.ac.uk, carmelita.carbone@inaf.it

Abstract. In recent years, the study of secondary anisotropies in the Cosmic Microwave Background has become a fundamental instrument to test our understanding of Cosmology and Astrophysics. Using a set of lightcones produced with the “Dark Energy and Massive Neutrino Universe” N -body simulations we study how different dark energy models and neutrino masses impact the properties of the Sunyaev-Zel'dovich (SZ) effects, focusing on the signal arising from galaxy clusters and groups. We analyse the distribution of values, Compton- y parameter for the thermal SZ effect and $\Delta T/T$ for the kinematic SZ effect, and study their angular power spectra. We find that the distribution of logarithmic Compton parameter can be fitted with a skewed Gaussian, with a mean that, at fixed dark energy model, decreases linearly with an approximate slope of $10f_\nu$. Regarding the power spectrum of the thermal SZ effect, we find that an increase in $\sum m_\nu$ is observed as a power-law scaling with respect to σ_8^{cb} , with exponents ranging from 7.2 to 8.2. We also find that four cosmological models, one with $\sum m_\nu = 0.16$ eV and three with $\sum m_\nu = 0.32$ eV, fit equally well the Planck data for the Compton- y . For all the DEMNUi models we forecast the cumulative signal-to-noise for thermal SZ observations with the LAT instrument of Simons Observatory; furthermore, we compute a tailored χ_{SNR}^2 estimator to infer if they can be distinguished from the reference Λ CDM. We also provide estimates for the power spectrum of the cluster component of the kinematic SZ effect, in all the different cosmological scenarios.

Keywords: Cosmology, Cosmic Microwave Background, Sunyaev-Zel'dovich effect, Neutrino, Dynamical Dark Energy

Contents

1	Introduction	1
2	The synthetic catalogues	2
2.1	The DEMNUni simulations	2
2.2	The halo catalogues	3
2.3	The creation of the lightcones	3
3	The Sunyaev-Zel’dovich effect	4
3.1	The tSZ model	5
3.2	The kSZ model (halo component)	6
3.3	The map-making process	6
4	Analysis of the tSZ effect	8
4.1	One-point statistics	8
4.2	Power spectrum	9
4.3	Forecasts of the Signal-To-Noise ratio	14
5	Analysis of the kSZ effect	15
5.1	One-point statistics	15
5.2	Power spectrum	17
6	Conclusions	19

1 Introduction

Since the earliest years of this century, measurements of the CMB anisotropies such as those from WMAP [1, 2], Planck [3–5] or ACT [6, 7] provided key estimates of different cosmological parameters. While for many probes the standard Λ CDM works excellently, in some cases tensions arise, leading to the necessity of extending the common Cosmological Framework (see e.g. the recent results from DESI [8]). In this work we investigate the extended models which make up the DEMNUni N-body simulation set [9, 10], characterized by the presence of massive neutrinos and a dynamical dark energy, through the Sunyaev-Zel’dovich effect. This effect has reached a role of key importance in Astrophysics and Cosmology, being nowadays routinely implemented in many diverse studies [11–17].

Key discoveries made at the end of the 90’s with detection experiments [18] led to the necessity of introducing a non-vanishing mass for neutrinos in the Standard Model of Particle Physics. For what concerns Cosmology, while massless neutrinos have been considered a fundamental ingredient in studies for many years, only in the last 10–15 years models with massive neutrinos became common in the analyses of different phenomena [5, 19–23]. In such scenarios, aside from variations in the neutrino background itself (for a treatment see [24] or, more extensively, [25]), there are changes in both the CMB and in the distribution of matter, depending at first order solely on the total mass of all neutrinos $M_\nu \equiv \sum m_\nu$, which has a lower bound of 0.06 eV imposed by flavour oscillation measurements [26]. As neutrinos interact only through gravity they constitute a collisionless fluid: one where there is no

bulk behaviour and no pressure propagation. In such fluids particles on average travel long distances in between interactions, and for neutrinos at low z this *mean free path* typically exceeds the scales of galaxy clusters, meaning that they can't be confined inside of them. This has a great impact on the Halo Mass Function (HMF), favouring smaller sized structures and almost erasing the very high-mass end, composed of the rarest clusters. This behaviour is known as free streaming, and significantly affects the observed (mostly thermal) SZ effect signal.

Regarding the nature of dark energy, the Chevallier-Polarski-Linder (CPL) [27, 28] is a popular model, which describes a dynamical dark energy fluid with equation of state (EoS) parametrized as

$$w(z) = w_0 + w_a \frac{z}{1+z} . \quad (1.1)$$

The cosmological constant Λ case can then be retrieved in the limit where $w_0 = -1$ and $w_a = 0$. This parametrization is of simple understanding and also solves problems that other choices might create, such as divergences at high redshift for the case of a linear $w(z)$.

This paper is structured as follows. In Section 2 we outline the simulation set and halo catalogues used for the analysis. In Section 3 we describe the Sunyaev-Zel'dovich effect, together with the pressure and density profiles utilized to characterize the electrons in the ICM and to create synthetic SZ maps. In Sections 4 and 5 we present the results of the analysis of the maps in all the different simulations. Lastly, in Section 6 we summarise the main findings.

2 The synthetic catalogues

2.1 The DEMNUni simulations

The simulation set used in this work is the “Dark Energy and Massive Neutrino universe” (DEMNUi): a total of 15 N-body simulations that implement the presence of massive neutrinos in a flat background with a dynamical dark energy. The DEMNUi have a large $2h^{-1}$ Gpc comoving size side box, filled with 2048^3 dark-matter particles (and 2048^3 neutrino particles, when present) evolving from $z = 99$ to $z = 0$. The simulations were run using the tree particle mesh-smoothed particle hydrodynamics code GADGET-3, an upgraded version of the one presented in [29], and are characterised by a softening length of $20h^{-1}$ kpc. The common cosmological parameters of the simulations are analogous to those resulting from the analysis of Planck 2013 [3] and shown in Table 1, together with the varied parameters. The presence of a dynamical dark energy was carried out using one of the four possible combinations of $w_0 = -0.9, -1.1$, $w_a = -0.3, +0.3$, in the language of the CPL parametrization. Concerning massive neutrinos, they were implemented in the simulations by using the modifications to GADGET-3 described in [30]. This improved version of the code treats the components of CDM and neutrinos separately, neglecting the calculation of the short-range tree force at early times for neutrinos, due to their high velocity dispersion and consequent large clustering scale. Furthermore, neutrinos are assumed to be in a degenerate mass scenario¹ with values of the total mass of $M_\nu = 0, 0.16, 0.32$ eV, and the budget for Ω_ν is taken from Ω_c .

¹Implying that all three mass eigenstates m_i have the same mass value.

No.	Type	$M_\nu \equiv 93.14 h^2 \Omega_\nu$ [eV]	Ω_c	(w_0, w_a)	$m_c^p [M_\odot h^{-1}]$	$m_\nu^p [M_\odot h^{-1}]$	$\sigma_8(z=0)$
1	Λ CDM	0	0.2700	$(-1, 0)$	8.27×10^{10}	-	0.830
2	$\nu\Lambda$ CDM	0.16	0.2662	$(-1, 0)$	8.17×10^{10}	9.97×10^8	0.793
3		0.32	0.2623		8.07×10^{10}	1.99×10^9	0.752
4	$w_0 w_a$ CDM	0	0.2700	$(-0.9, -0.3)$	8.27×10^{10}	-	0.828
5				$(-0.9, +0.3)$			0.777
6				$(-1.1, -0.3)$			0.861
7				$(-1.1, +0.3)$			0.831
8	$\nu w_0 w_a$ CDM	0.16	0.2662	$(-0.9, -0.3)$	8.17×10^{10}	9.97×10^8	0.791
9				$(-0.9, +0.3)$			0.742
10				$(-1.1, -0.3)$			0.822
11				$(-1.1, +0.3)$			0.794
12		0.32	0.2623	$(-0.9, -0.3)$	8.07×10^{10}	1.99×10^9	0.750
13				$(-0.9, +0.3)$			0.705
14				$(-1.1, -0.3)$			0.780
15				$(-1.1, +0.3)$			0.753

Table 1: Cosmological parameter values of the DEMNUni simulation suite. The reference cosmology for all the models has $\{\Omega_b, \Omega_m \equiv \Omega_c + \Omega_b + \Omega_\nu, h, n_s, A_s\} = \{0.05, 0.32, 0.67, 0.96, 2.1265 \times 10^{-9}\}$. Above we show only the values of the varied parameters for the different cosmological scenarios considered in this work.

2.2 The halo catalogues

For each simulation a total of 63 outputs were produced, logarithmically equispaced in the redshift range considered. Each of those outputs was processed first with a **Friends of Friends** (FoF) algorithm with a linking length of 0.2, and subsequently with the **Subfind** algorithm, both already included in **GADGET-3** [31, 32]. These allow the correct identification of gravitationally bound structures, and produce catalogues of haloes each with its mass, position and (peculiar) velocity. While the initial catalogues included haloes down to $M_{200} = 2.5 \times 10^{12} h^{-1} M_\odot$, we applied a cut in mass at $M_{200} = 3.4 \times 10^{13} h^{-1} M_\odot$ to save computational time. We verified that this has a negligible impact on our main findings, related to the power spectrum of the thermal SZ effect (as we will see in Section 4).

2.3 The creation of the lightcones

To obtain *mock* universes from the DEMNUni halo catalogues and use them to study the SZ effect, it is necessary to create full-sky backward lightcones. The construction of the halo lightcone follows a procedure similar in its geometrical approach to the one employed for CMB lensing (CMBL) maps, as described in [33, 34] and validated in [35, 36]. In this case, instead of dark matter particles, the halo catalogue is extracted from the DEMNUni simulations using the **Subfind** algorithm and placed within a full-sky, 3D framework around a central observer. The methodology involves replicating the finite simulation volume to cover the entire past lightcone up to a chosen redshift, ensuring a continuous structure along the line of sight. Specifically, the volume is divided into concentric spherical shells of fixed comoving thickness, within which all simulation outputs are subjected to coherent translations and rotations, rather than independent random transformations. This approach, originally developed for weak lensing applications, preserves the continuity of the gravitational potential across transverse

directions. The resulting halo lightcones extend to a maximum redshift of $z_{\max} \approx 2.5$, aligning with the redshift range relevant for the Euclid mission [37]. Each halo within this framework is characterized by ten parameters, namely its mass M_{200} , angular coordinates, comoving distance, Cartesian position, and peculiar velocity. This process is applied to all simulations, yielding full-sky, 3D halo catalogues across the multiple cosmological scenarios shown in Table 1.

3 The Sunyaev-Zel’dovich effect

The SZ effect is a source of CMB secondary anisotropies, emerging due to the Compton scattering of the radiation off ionised electrons [38–41]. The thermal random motion of the electrons leads to a specific temperature variation in the spectrum of the CMB, given by

$$\frac{\Delta T_{\text{CMB}}}{T_{\text{CMB}}} = y \left(\frac{x}{\tanh x/2} - 4 \right) \equiv y g(x) , \quad (3.1)$$

where

$$x \equiv \frac{h\nu}{k_{\text{B}} T_{\text{CMB}}} , \quad (3.2)$$

$$y \equiv \frac{\sigma_{\text{T}}}{m_{\text{e}} c^2} \int_0^\infty d\lambda n_{\text{e}} k_{\text{B}} T_{\text{e}} = \frac{\sigma_{\text{T}}}{m_{\text{e}} c^2} \int_0^\infty d\lambda P_{\text{e}}(\lambda) . \quad (3.3)$$

m_{e} , σ_{T} and k_{B} are respectively the electron mass, the Thompson cross-section and the Boltzmann constant, while c is the light speed in vacuum. The quantities n_{e} , T_{e} and P_{e} are number density, temperature and pressure of the electron gas. The variable x is the *dimensionless frequency*, while y , better known as Compton parameter, is a measure of the integrated electron pressure along the physical line of sight λ . This is the thermal SZ effect (tSZ).

On the other hand, ionised electrons also possess a non-zero velocity that leads to an additional, frequency independent, variation in the CMB temperature:

$$\frac{\Delta T_{\text{CMB}}}{T_{\text{CMB}}} = - \int_0^\infty d\lambda n_{\text{e}} \sigma_{\text{T}} e^{-\tau} \frac{v_{\text{los}}}{c} . \quad (3.4)$$

In the above τ is the optical depth for Compton scattering, while v_{los} is the proper velocity of the electron plasma along the line of sight. This is the kinematic, or kinetic, SZ effect (kSZ). Our analysis, which focuses solely on the component of galaxy clusters and groups, makes for an excellent approximation of the tSZ effect; this happens since it is sourced by the energy density of ionised electrons, which is most prominent inside large bound structures due to their deep gravitational potential wells. In turn, since the kSZ effect does not depend directly on the electron temperature, it receives a significant contribution from the gas in non-virialised structures at temperature between 10^5 and 10^7 K and would require a more sophisticated treatment with hydrodynamical simulations (see [20, 42] and references therein). A precise estimate of the kSZ effect and its dependence with cosmology is therefore beyond the scope of this work. Nonetheless, with the DEMNUni simulations we can define a modelling of the halo component of the kSZ signal that we describe in Section 3.2: therefore its prediction has to be regarded as an underestimate of the true one.

3.1 The tSZ model

We model the gas pressure in the selected haloes using the Battaglia profile

$$P(X) = P_{200} P_0 (X/x_c)^\gamma [1 + (X/x_c)^\alpha]^{-\beta} , \quad (3.5)$$

resulting from the hydrodynamical simulations described in [43]. Here $X \equiv r/R_{200}$, while α and γ are fixed respectively to the values 1.0 and -0.3 . The other 3 parameters P_0 , x_c and β vary with respect to M_{200} and z (see [43] for an accurate description). We stress here that the overdensity threshold, set equal to 200, has to be intended with respect to the *critical* density ρ_{cr} . The scale value P_{200} is the self-similar pressure given by

$$P_{200} = GM_{200} 200\rho_{\text{cr}}(z) \frac{1}{2R_{200}} f_b , \quad (3.6)$$

where f_b is the ratio of baryonic matter with respect to total matter in the halo. We compute this ratio as

$$f_b = \frac{\Omega_b}{\Omega_m - \Omega_\nu} \quad (3.7)$$

to account for the free-streaming of neutrinos. In Eq. (3.6) the values of M_{200} and R_{200} are taken individually for each galaxy cluster/group from our halo catalogues (Section 2.2), while the value of f_b is fixed for every cosmological model: with the 3 different M_ν in the simulations (see Table 1) we obtain the values 0.1563, 0.1581, 0.1601. This follows from the fact that, in a scenario with fixed Ω_m and Ω_b as in the DEMNUni case, haloes with the same mass have increasingly higher baryon content with greater M_ν . We show examples of the resulting pressure profiles in Figure 1. Once the total gas pressure is defined, the electron pressure is obtained assuming a pristine cosmological gas in full ionization, through

$$P_e = \frac{2(f_H + 1)}{(5f_H + 3)} P \simeq 0.52 P , \quad (3.8)$$

where $f_H = 0.76$ is the primordial hydrogen mass fraction.

In Sections 4 and 5 we compute the power spectrum of both the tSZ and kSZ effects, calibrating the process by comparing the tSZ results to the theoretical expectations of the halo model in the Λ CDM scenario. In the small scale, $\ell \gg 1$, limit this power spectrum has the following 1-halo and 2-halo terms [44, 45]:

$$C_\ell^{1h} = \int_{z_{\min}}^{z_{\max}} dz \frac{d^2V}{d\Omega dz} \int_{M_{\min}}^{M_{\max}} dM n(M, z) |\tilde{y}_\ell(M, z)|^2 , \quad (3.9)$$

$$C_\ell^{2h} = \int_{z_{\min}}^{z_{\max}} dz \frac{d^2V}{d\Omega dz} \left[\int_{M_{\min}}^{M_{\max}} dM n(M, z) \tilde{y}_\ell(M, z) B(M, z) \right]^2 P_m(k, z) . \quad (3.10)$$

Here V is the comoving volume, $n(M, z)$ is the HMF, $P_m(k = (\ell + 1/2)/d_C, z)$ is the matter linear power spectrum and $B(M, z)$ the linear halo bias. The profile $\tilde{y}_\ell(M, z)$ is the 2-dimensional Fourier transform of the Compton parameter

$$\tilde{y}_\ell(M, z) = \frac{4\pi r_c}{\ell_c^2} \frac{\sigma_T}{m_e c^2} \int_0^\infty ds s^2 P_e(s, M, z) \frac{\sin(\ell s/\ell_c)}{(\ell s/\ell_c)} , \quad (3.11)$$

in which r_c is the scale radius of the pressure profile P_e , $s = r/r_c$ and $\ell_c = d_A/r_c$.

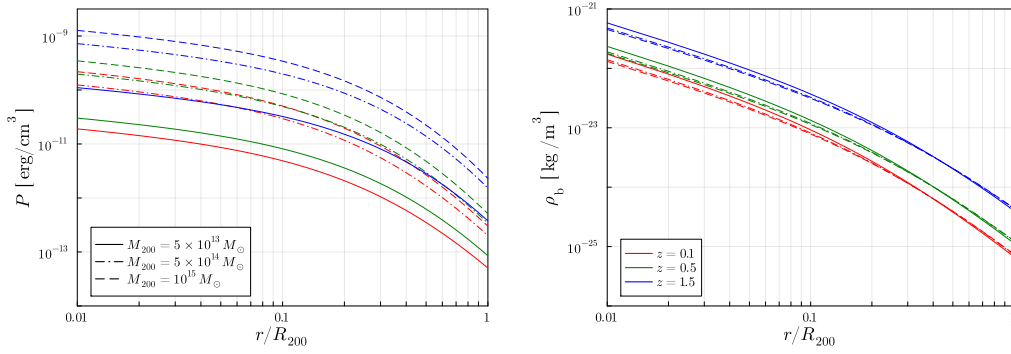


Figure 1: LEFT: Battaglia pressure profile of Equation (3.5), as a function of r/R_{200} , for different redshifts and M_{200} . RIGHT: NFW profile for the baryon density ρ_b of Equation (3.12), as a function of r/R_{200} , for the same z , M_{200} combinations. The cosmological parameters for both are the ones of the Λ CDM simulation.

3.2 The kSZ model (halo component)

We model the density of baryons inside the haloes with an NFW [46] profile

$$\rho_b(r) = (1 - f_*)f_b \rho(r) = (1 - f_*)f_b \frac{\rho_0}{(r/r_s)(1 + r/r_s)^2}, \quad (3.12)$$

where f_* is the stellar mass fraction, that we fix to 0.1. We account for the dependencies of r_s and ρ_0 on M_{200} and z through the Duffy concentration parameter

$$R_{200}/r_s \equiv c_{200} = 5.71 \left(\frac{M_{200}}{2 \times 10^{12} h^{-1} M_\odot} \right)^{-0.084} (1 + z)^{-0.47}, \quad (3.13)$$

derived from N-body simulations [47], retrieving ρ_0 by normalising $\rho(r)$ to M_{200} at R_{200} . The resulting density profiles are also shown in Figure 1. The electron density can then be computed by rescaling the baryon density as

$$n_e = \frac{1}{\mu m_p} \rho_b, \quad (3.14)$$

where $\mu = [f_H + \frac{1}{2}(1 - f_H)]^{-1} \simeq 1.14$ is the mean molecular weight per electron of a fully ionised cosmological gas in units of the proton mass m_p . Finally, the kSZ induced CMB temperature variation is derived for each halo with Equation (3.4), considering the density profile as in Eq. (3.14) and v_{los} taken for each halo from their individual peculiar velocities, as extracted from the catalogues (Section 2.2), thus neglecting internal motions. Since we are considering objects at relatively low redshift ($z < 2.5$) we can safely assume $\exp(-\tau) \simeq 1$.

3.3 The map-making process

Once defined the models describing the pressure and number density of the electrons, we apply them to the 15 halo lightcones deriving from the DEMNUni set (see Section 2). For each halo we integrate the relevant quantities along the lines of sight within a radius of $4R_{200}$ from its centre, to obtain estimates for Compton- y (tSZ) and for $\Delta T/T$ (kSZ). By summing, in each direction in the sky, the contribution from all haloes we are able to create the synthetic

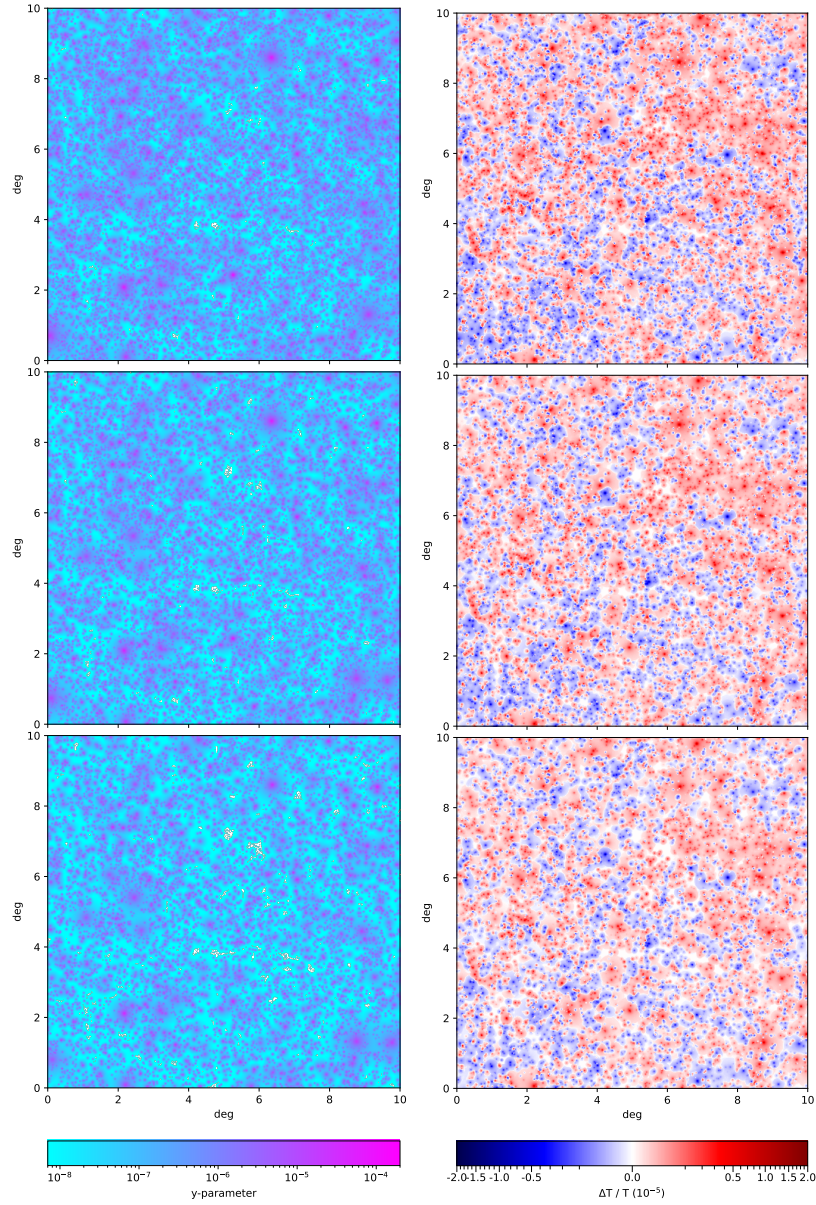


Figure 2: Example of three synthetic maps of Compton- y parameter for the tSZ (left column) and of relative temperature change for the kSZ (right column) in the cosmological constant DEMNUni models, with M_ν increasing from top to bottom (respectively number 1, 2 and 3 in Table 1). In the maps it is possible to see many massive haloes, with y values up to 10^{-4} and $\Delta T^{\text{kSZ}}/T$ reaching approximately $\pm 10^{-5}$. While the analysis described in Sections 4 and 5 is done using full-sky maps, here we only show a patch of $10^\circ \times 10^\circ$ selected near the equator, to avoid the visual deformation at the poles induced by the CAR pixelisation scheme.

SZ maps. For this purpose we use the code **XGPaint**², which was specifically developed to paint emission of extragalactic foregrounds on dark matter halos. As our baseline choice we produce our maps in the CAR pixelisation scheme [48]. We choose to generate, for each

²<https://websky-cita.github.io/XGPaint.jl/stable/>

of the two effects and each of the simulations, two types of map:

- a full-sky, lower resolution (with a pixel size of 0.5°) one, for the one-point statistics;
- a full-sky, higher resolution (with a pixel size of $0.5'$) one, for the computation of the power spectrum.

We show examples of smaller maps in Figure 2. It is possible to see how the presence of massive neutrinos lowers the signal for both the effects, but more markedly for the tSZ. Nonetheless, the formed structures appearing in the different maps resemble each other, highlighting the specific imprint of free streaming.

4 Analysis of the tSZ effect

4.1 One-point statistics

For the analysis of the one-dimensional pixel distribution of the tSZ effect we choose to work with $\log(y)$ rather than y itself, as the ensemble of values spans different orders of magnitude, approximately from 10^{-9} to 10^{-4} . Before working in logarithmic scale every null pixel in the map was removed: these are associated to a lack of contribution in the region by haloes, implying that the line of sight associated to the pixel is not within a distance of $4R_{200}$ from the centre of any structure, and are present in our mock maps due to the absence of a modelling for the diffuse gas. These $y = 0$ pixels amount to around 3% to 10% of the map, depending on the chosen simulation. The resulting $\log(y)$ distributions can be fitted with a skewed Gaussian [49]:

$$P(x) = \frac{2}{\sigma\sqrt{2\pi}} e^{-\frac{(x-\mu)^2}{2\sigma^2}} \int_{-\infty}^{\alpha \frac{x-\mu}{\sigma}} dt \frac{1}{\sqrt{2\pi}} e^{-\frac{t^2}{2}}, \quad (4.1)$$

where μ and σ represent the standard Gaussian mean and variance, while α is the parameter quantifying the skewness. The results of the fitting for α and σ are listed in Table 2, while in Figure 3 we compare the actual distributions to the best-fitting curves in the Λ cosmological models. In all cases an increase in neutrino mass, with fixed dark energy EoS, leads to larger values both for σ and α . The latter, in particular, is always positive, meaning that the distribution favours values larger than the one corresponding to the peak, and its increment with greater M_ν can be explained in the following way: more massive neutrinos lead to a downward shift in the HMF, coupling this with a fixed mass cut favours the presence of greater y as they are derived from more massive haloes.

We then look more in detail at the mean $\log(y)$ (shown in Figure 4) and its trend when varying M_ν . As expected, for a fixed dark energy EoS, an increase in neutrino mass translates to a decrement in the mean logarithmic value. What is more interesting is that this trend is mostly linear and so it can be fitted as

$$\langle \log(y) \rangle = A_1 + A_2(1 - f_\nu), \quad (4.2)$$

with $f_\nu \equiv \Omega_\nu/\Omega_m$ being the neutrino mass fraction. The best-fit values of A_1, A_2 for the different dark energy EoS combinations are also presented in Figure 4, and correspond to a standard deviation of order 10^{-2} or less. Very interestingly, the observed reduction of approximately $10f_\nu$ is analogous to the nonlinear damping in the matter power spectrum caused by massive neutrinos [9].

Simulation		α	σ
$M_\nu = 0 \text{ eV}$	$w_0 = -1, w_a = 0$	0.88	0.84
	$w_0 = -0.9, w_a = -0.3$	0.88	0.84
	$w_0 = -0.9, w_a = +0.3$	1.16	0.92
	$w_0 = -1.1, w_a = -0.3$	0.78	0.80
	$w_0 = -1.1, w_a = +0.3$	0.88	0.83
$M_\nu = 0.16 \text{ eV}$	$w_0 = -1, w_a = 0$	1.05	0.89
	$w_0 = -0.9, w_a = -0.3$	1.06	0.89
	$w_0 = -0.9, w_a = +0.3$	1.40	0.97
	$w_0 = -1.1, w_a = -0.3$	0.91	0.84
	$w_0 = -1.1, w_a = +0.3$	1.05	0.89
$M_\nu = 0.32 \text{ eV}$	$w_0 = -1, w_a = 0$	1.35	0.96
	$w_0 = -0.9, w_a = -0.3$	1.34	0.96
	$w_0 = -0.9, w_a = +0.3$	1.77	1.04
	$w_0 = -1.1, w_a = -0.3$	1.15	0.91
	$w_0 = -1.1, w_a = +0.3$	1.33	0.96

Table 2: α and σ parameters for the skewed Gaussian distribution (Equation 4.1) best-fit, for each of the 15 DEMNUni simulations.

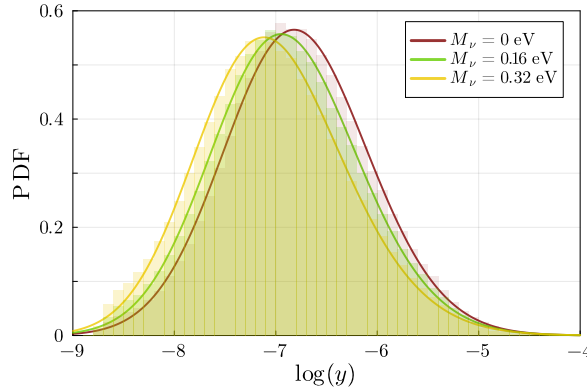


Figure 3: Normalised distribution of the Compton parameter (in logarithmic scale) for the three M_ν values in the cosmological constant simulations (number 1, 2 and 3 in Table 1). The best-fitting skewed Gaussian is also plotted.

4.2 Power spectrum

We obtain the angular power spectra of Compton- y by directly decomposing the signal over the spherical harmonics basis in the higher resolution ($0.5'$) maps. The computation is affected by numerical error, which we can not smooth out averaging over more realisations because for each simulation only one lightcone is produced. We therefore apply a moving average method over 11 multipoles

$$\langle C_\ell \rangle = \frac{1}{11} \sum_{\ell-5}^{\ell+5} C_\ell, \quad (4.3)$$

to produce a smoothed version of all the power spectra to show in the figures. To first test our calculation we compare, in the Λ CDM model, the DEMNUni results and the halo

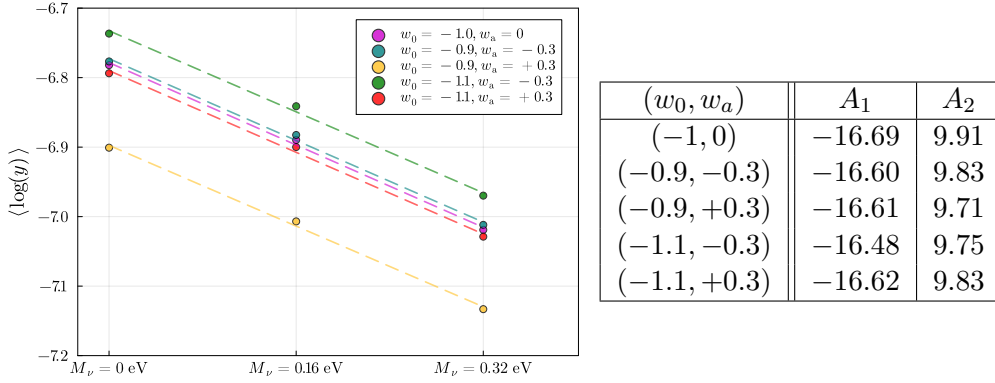


Figure 4: Mean $\log(y)$ values for all the DEMNUni simulations, together with the linear fit of Equation (4.2) for each dark energy EoS (the associated parameters are listed on the right). Notice how in the $(w_0 = -0.9, w_a = +0.3)$ models, which are the ones where dark energy contributes the most, the mean $\log(y)$ values are significantly lower.

model expectations from CLASS_{sz} [50, 51]. The latter is computed setting all the cosmological parameters equal to those of the DEMNUni simulations and using the Tinker halo mass function and bias [52]. We set the maximum redshift to 2.5 as in our lightcones, as well as a minimum mass of $3.4 \times 10^{13} h^{-1} M_\odot$ for the integration in Equations (3.9) and (3.10). The results of this comparison, for different low- z cuts, are shown in Figure 5. This comparison highlights differences between the two approaches both for $\ell \lesssim 300$ and $\ell \gtrsim 3000$: while for large scales the potential reason of this discrepancy is the single lightcone realisation coupled with the finite simulation volume³, for the differences at the smallest scales (which at $\ell = 10^4$ consists of 20% more power in the simulations compared to the halo model from CLASS_{sz}) we haven't found a reasonable explanation. Increasing the resolution does not solve the issue, as the effects of the pixelisation appear only for $\ell > 10^4$; we find that only by selecting the whole mass sample (without the $3.4 \times 10^{13} h^{-1} M_\odot$ mass cut) the discrepancy disappears. In fact, both calculations in this scenario have an increased power for $\ell \gtrsim 3000$, more marked for CLASS_{sz} so that it matches the results for the DEMNUni lightcone, which, in contrast, shows only a slight increase. But this approach is both computationally unfeasible and unphysical, as the pressure model is suited only for galaxy clusters and groups, so we keep the mass cut. We also decide to select only haloes at $z > 0.05$, so to have a better statistical description of the phenomenon by avoiding local effects, but at the same time significantly reducing power at the larger scales.

The power spectra of all the simulations, computed with the previous specifications, are shown in Figure 6. It is possible to see how both a dynamical dark energy and massive neutrinos greatly impact the outcome. Their effect at first order is similar, almost degenerate, resulting in a rescaling of the tSZ power. While this is true at all scales of interest for massive neutrinos, a dynamical dark energy impacts differently the $\ell \gtrsim 2000$ region, where the power spectra (at fixed M_ν) with $(w_0, w_a) = (-0.9, +0.3), (-1.1, -0.3), (-1.1, +0.3)$ ultimately converge at $\ell = 10^4$. For each neutrino mass the range covered by the power spectra in all the possible dark energy EoS is larger at $\ell = 100$ than at $\ell = 10^4$ by approximately 60, 63, 56%, respectively for $M_\nu = 0, 0.16, 0.32$ eV. At fixed M_ν , in the $\ell \lesssim 2000$ range there is little

³Which limits the power at large scales due to the replication of the same box.

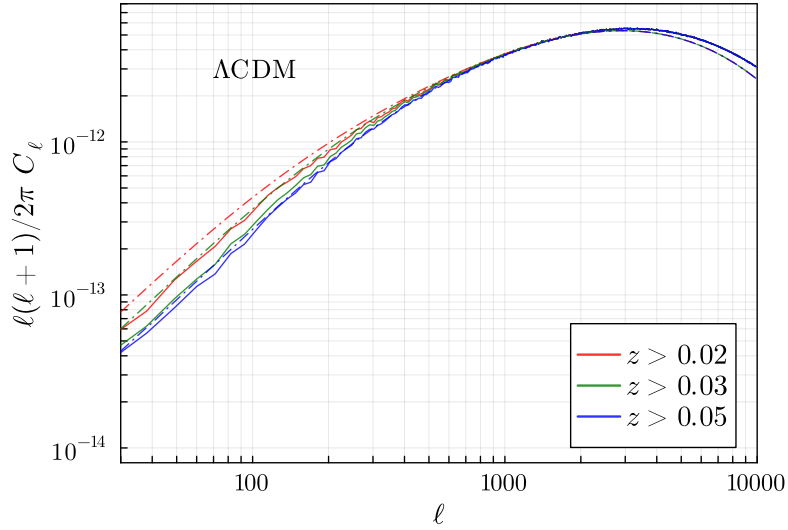


Figure 5: Comparison of the tSZ effect power spectrum in the Λ CDM scenario between the DEMNUi calculation (solid) and CLASS_{sZ} (dash-dotted), with different low- z cuts. We always show the power spectra of the tSZ for $\Delta T/T$, obtained in the low frequency limit where $g(x) \rightarrow -2$ (see Eq. (3.1)).

difference between the $(w_0, w_a) = (-1, 0), (-0.9, -0.3), (-1.1, +0.3)$ models, with instead the $(w_0, w_a) = (-0.9, +0.3), (-1.1, -0.3)$ curves remaining respectively lower and higher. Simulations with massless neutrinos tend to strongly overestimate the Planck [54] data from [53], particularly at the smaller scales. To better quantify the adherence of each cosmological model with the data we calculate a reduced χ^2 , defined as

$$\chi^2 = \frac{1}{N_{\text{points}}} \sum_{\tilde{\ell}} \frac{(C_{\tilde{\ell}} - C_{\tilde{\ell}}^{\text{data}})^2}{(\sigma_{\tilde{\ell}}^{\text{data}})^2}, \quad (4.4)$$

for $\tilde{\ell} > 300$ modes, where $\tilde{\ell}$ indicates the multipole of each data point and $C_{\tilde{\ell}}$ is calculated as in (4.3). Selecting only $\tilde{\ell} > 300$ ensures we avoid the region affected by our cut at $z = 0.05$. Here we assume the data points to be independent from each other, leading to an incorrect estimate of the actual χ^2 due to the neglect of the full covariance matrix. This nonetheless gives a useful assessment of how close each curve is to the binned data points. The results are listed in Table 3 and show that four simulations have a clearly lower discrepancy with the data compared to the others:

- $M_\nu = 0.16$ eV ($w_0 = -0.9, w_a = +0.3$);
- $M_\nu = 0.32$ eV ($w_0 = -1, w_a = 0$);
- $M_\nu = 0.32$ eV ($w_0 = -0.9, w_a = -0.3$);
- $M_\nu = 0.32$ eV ($w_0 = -1.1, w_a = +0.3$).

We also explore the share of power in different redshift intervals, which we choose to be $0.05 < z < 0.5$, $0.5 < z < 1$ and $z > 1$. This is done to investigate a potential different

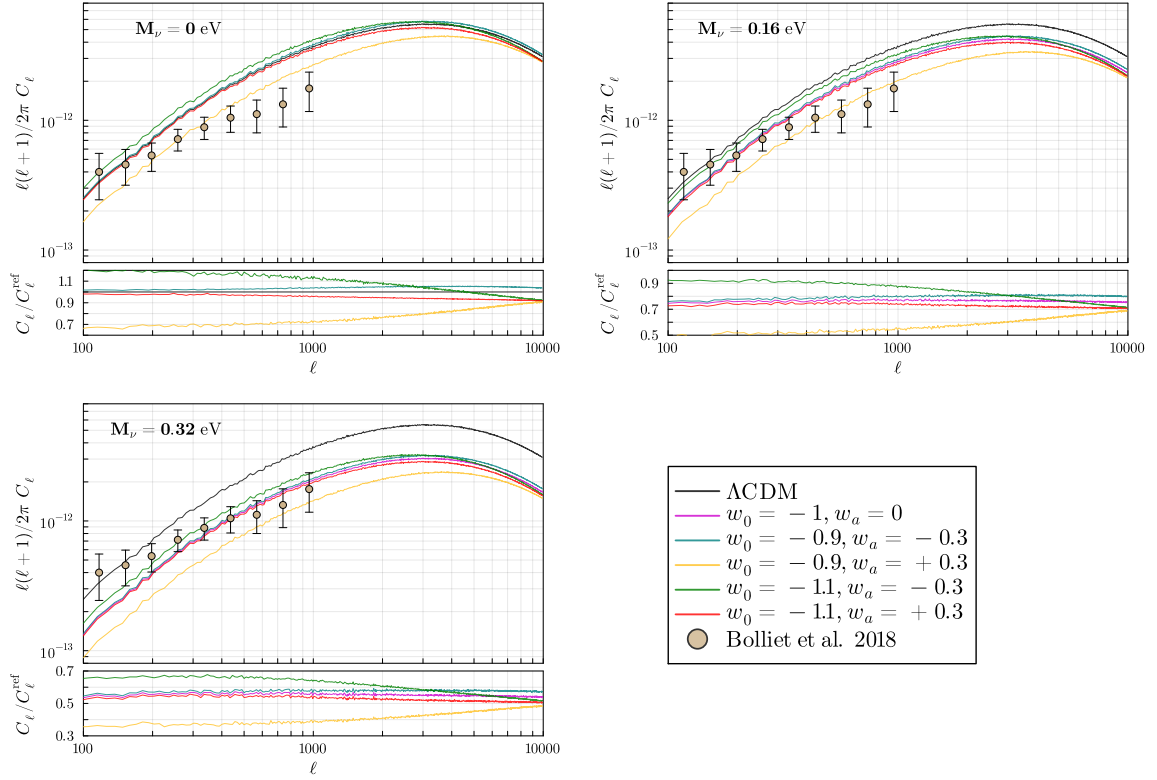


Figure 6: Power spectra for the tSZ effect in the DEMNUni simulations, compared with the Planck data from [53]. Top-left are the massless cases, while top-right and bottom correspond respectively to $M_\nu = 0.16$ eV and $M_\nu = 0.32$ eV; all of these are evaluated for $z > 0.05$. The ratio of each power spectrum with respect to the reference Λ CDM simulation is also present in the panels.

redshift dependence between the 15 scenarios, mainly due to the variability in the EoS for dark energy, which is *not* observed. In fact, all the DEMNUni models show the same trend: up to $\ell = 3000$ the dominant slice is $z < 0.5$, while at $\ell \approx 10^4$ z_2 and z_3 each amount to 40–50% of the power of the whole redshift sample (see Figure 7).

Furthermore, we investigate the scaling of the power spectrum, in the interval $300 < \ell < 1000$, with respect to $\sigma_8(z=0)$, calculated via CAMB [55, 56], and Ω_m , parameters to which the tSZ effect is very sensitive. The steepest dependence is expected to be on σ_8 , as it is a measure of the amount of clustering today, with typical values in the literature being $C_\ell \propto \sigma_8^{7-9}$ [54, 57–60]. The authors of [60] stressed the importance of the ‘cb’ prescription when in presence of massive neutrinos [61, 62], that is to say using the same parametrisation of the HMF [63] as in massless neutrino cosmological models

$$n(M, z) = \frac{\rho_m}{M} f(\sigma, z) \frac{d \ln \sigma^{-1}}{d \ln M} , \quad (4.5)$$

but with the density and variance evaluated only for baryons and CDM, so $\rho_{\text{cb}} = \rho_m - \rho_\nu$ and σ^{cb} . This prescription reflects the effects of neutrino free-streaming and should allow precise estimates of $n(M, z)$ by calibrating $f(\sigma, z)$ purely in massless neutrinos simulations.

Simulation		Reduced χ^2 ($\tilde{\ell} > 300$)
$M_\nu = 0 \text{ eV}$	$w_0 = -1, w_a = 0$	12.17
	$w_0 = -0.9, w_a = -0.3$	13.60
	$w_0 = -0.9, w_a = +0.3$	1.97
	$w_0 = -1.1, w_a = -0.3$	21.44
	$w_0 = -1.1, w_a = +0.3$	10.55
$M_\nu = 0.16 \text{ eV}$	$w_0 = -1, w_a = 0$	3.35
	$w_0 = -0.9, w_a = -0.3$	3.95
	$w_0 = -0.9, w_a = +0.3$	$^\dagger 0.35$
	$w_0 = -1.1, w_a = -0.3$	7.72
	$w_0 = -1.1, w_a = +0.3$	2.75
$M_\nu = 0.32 \text{ eV}$	$w_0 = -1, w_a = 0$	$^\dagger 0.34$
	$w_0 = -0.9, w_a = -0.3$	$^\dagger 0.41$
	$w_0 = -0.9, w_a = +0.3$	1.55
	$w_0 = -1.1, w_a = -0.3$	1.16
	$w_0 = -1.1, w_a = +0.3$	$^\dagger 0.28$

Table 3: Reduced χ^2 for the DEMNUni simulations power spectra with the data from [53], for $\tilde{\ell} > 300$. Daggers indicate the best-fitting, lower χ^2 values.

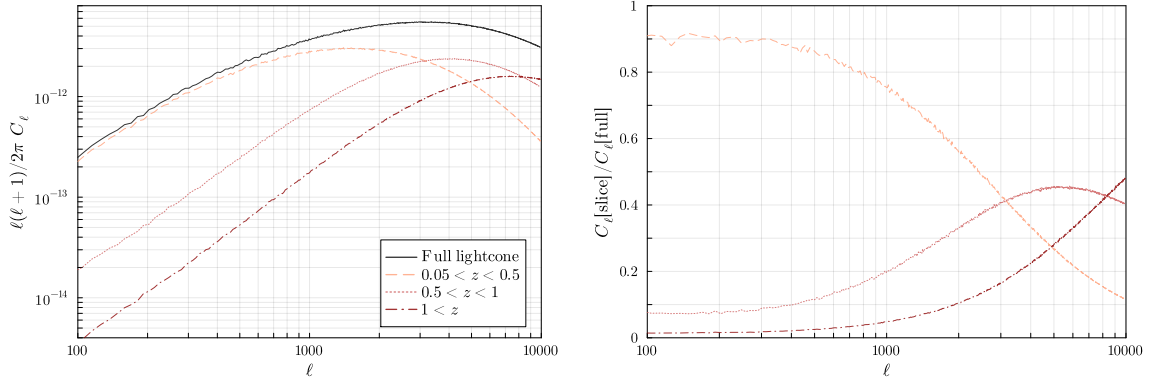


Figure 7: Power spectrum of the tSZ effect in the the three different redshift slices, compared to the full lightcone calculation, in the DEMNUni Λ CDM simulation. The behaviour in the the other 14 simulations is analogous to the Λ CDM one, with no major differences.

We accordingly focus on the ‘cb’ quantities. Also, a separate analysis of pure σ_8^{cb} scaling with fixed Ω_{cb} can’t be done with the DEMNUni simulations. That is because it would imply looking at a varying dark energy EoS with fixed M_ν , so that the direct proportionality between the number of massive haloes (which are the main source of the tSZ effect) and the value of σ_8^{cb} is spoiled as different (w_0, w_a) combinations lead to a different pattern of structure formation. Therefore this parameter is unable to trace the variation of the C_ℓ spectrum when two diverse dynamical dark energy EoS are considered. As an example, for better clarity: for each M_ν the $(w_0 = -0.9, w_a = -0.3)$ simulation shows more power when compared to the cosmological constant scenario (see again Figure 6) but present smaller values of σ_8^{cb} . We therefore analyse the scaling varying only M_ν and keeping fixed (w_0, w_a) , meaning that both σ_8^{cb} and Ω_{cb}

(w_0, w_a)	q
$(-1, 0)$	7.5
$(-0.9, -0.3)$	7.5
$(-0.9, +0.3)$	8.2
$(-1.1, -0.3)$	7.2
$(-1.1, +0.3)$	7.5

Table 4: Power-law exponent for the scaling of the tSZ effect power spectrum with respect to σ_8^{cb} only, obtained keeping a fixed dark energy EoS while varying M_ν .

change simultaneously. But the latter varies minimally in the DEMNUni set⁴, so we choose to neglect its impact on the power spectrum and focus on σ_8^{cb} only:

$$C_\ell \propto (\sigma_8^{\text{cb}})^q . \quad (4.6)$$

This results in 5 values for q presented in Table 4. Even though our simulation-based scaling is obtained by fitting only a limited number of curves (and also neglecting the small Ω_{cb} contribution), the q values we find differ from those used in [53, 60]. We therefore suggest that future work should take care in assuming a fixed scaling relation with the cosmological parameters, having shown in the case of σ_8^{cb} how the relation itself is dependent on the pressure profile choice and on the nature of dark energy.

4.3 Forecasts of the Signal-To-Noise ratio

Here we provide the forecast for the signal-to-noise ratio (SNR) for the detection of the tSZ effect, specifically regarding the observations with the LAT instrument of Simons Observatory (SO) [64]. The SNR computation starts by evaluating the covariance matrix

$$\mathcal{M}_{\ell\ell'} = \frac{1}{4\pi f_{\text{sky}}} \left(4\pi\delta_{\ell\ell'} \frac{2(C_\ell + N_\ell)^2}{2\ell + 1} + T_{\ell\ell'} \right) , \quad (4.7)$$

where N_ℓ is the noise power spectrum (after the removal of any foreground) and $T_{\ell\ell'}$ is the tri-spectrum for the tSZ [45, 65], while f_{sky} is the fraction of the sky covered (equal to 0.4 for SO). The tri-spectrum gives a non negligible non-Gaussian contribution up to moderate ℓ (see e.g. [66]), but it can be suppressed by eliminating the most massive clusters [45, 60]. As the calculation of the tri-spectrum can be rather tedious we decide to apply such procedure, more specifically cutting at $3.4 \times 10^{14} h^{-1} M_\odot$. Doing so leads to new values for the power spectra, which are inevitably lower but provide a more accurate signal-to-noise estimate, and to a purely Gaussian covariance

$$\mathcal{M}_\ell = \frac{2}{f_{\text{sky}}(2\ell + 1)} (C_\ell + N_\ell)^2 . \quad (4.8)$$

For what concerns the noise, we opt for the one obtained by SO collaboration by constraining both CMB and CIB, which constitutes the least optimistic but more realistic option, ranging from $\ell = 80$ to $\ell = 7979$ (see Figure 8). Once the covariance matrix has been estimated with N_ℓ , the corresponding *cumulative* signal-to-noise ratio is given by

$$\text{SNR}(\ell_{\text{max}}) = \sqrt{\sum_{\ell, \ell'}^{\ell_{\text{max}}} \frac{C_\ell C_{\ell'}}{\mathcal{M}_{\ell\ell'}}} \stackrel{\text{Gauss.}}{=} \sqrt{\sum_{\ell}^{\ell_{\text{max}}} \frac{C_\ell^2}{\mathcal{M}_\ell}} . \quad (4.9)$$

⁴The values of Ω_{cb} are 0.32, 0.3162, 0.3123.

The cumulative SNR results are plotted in Figure 9. If the masking of the more massive haloes can be obtained, Simons Observatory should reach values up to $15 \lesssim \text{SNR} \lesssim 27.5$ for observations of the tSZ effect. Due to the specific shapes of both the signal and the noise power spectrum the crucial interval for obtaining a significative signal-to-noise is approximately (1500, 6000), after which the SNR values stabilize.

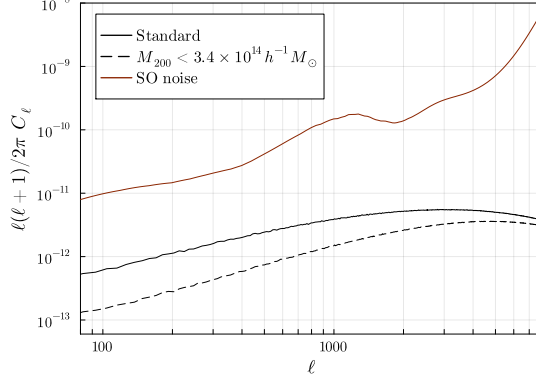


Figure 8: Simons Observatory LAT noise model and DEMNUni Λ CDM tSZ power spectra compared. For the latter there are both our standard calculation and the one with the $3.4 \times 10^{14} h^{-1} M_\odot$ cut. The noise is the same as the dotted orange line in Figure 36 of [64], here shown in the low frequency limit.

Besides, with the same formalism described above, it is possible to quantify the detectability of deviations from a certain reference cosmological model [67]. This is done by substituting the C_ℓ 's at the numerator in Equation (4.9) with

$$\Delta C_\ell = C_\ell^{\text{ref}} - C_\ell, \quad (4.10)$$

i. e. the difference between the power spectra calculated respectively in the reference model and in the model investigated; then we calculate the signal-to-noise χ^2 with

$$\chi_{\text{SNR}}^2 = \sum_{\ell}^{\ell_{\text{max}}} \frac{\Delta C_\ell^2}{\mathcal{M}_\ell^{\text{ref}}}, \quad (4.11)$$

where the covariance is meant to be evaluated for the reference scenario. We use this estimator to probe whether the different cosmological models characterising the DEMNUni set could be potentially distinguished from the reference Λ CDM with statistical significance with data of the tSZ effect from Simons Observatory. In Figure 9 we show the results obtained for $\sqrt{\chi^2}$, in analogy to the cumulative SNR. Assuming that the detection is only possible at more than 5σ 's, we conclude that SO will be able to discriminate between Λ CDM and cosmologies with $M_\nu = 0.32$ eV, as well as most of those with $M_\nu = 0.16$ eV (aside from the $(w_0, w_a) = (-0.9, -0.3)$ one), but not between different dark energy EoS in a massless neutrino scenario.

5 Analysis of the kSZ effect

5.1 One-point statistics

Looking first at the right column of Figure 2, it is possible to appreciate the symmetric nature of the kSZ signal, even on a small fraction of the sky, which is due to the nature of

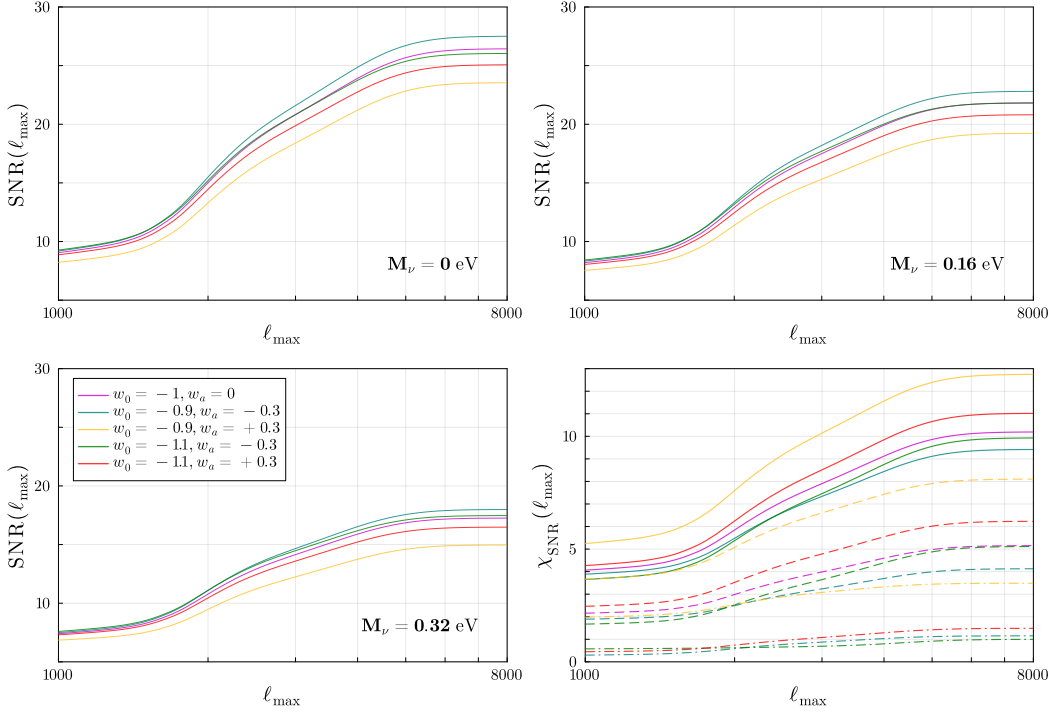


Figure 9: Cumulative signal-to-noise ratio for observations with the SO LAT instrument for the tSZ effect, as calculated from the different **DEMUNi** simulations. Top-left, top-right and bottom-left are respectively $M_\nu = 0, 0.16, 0.32$ eV. In the bottom-right plot we show the χ^2 of Equation (4.11), with respect to the reference Λ CDM simulation: dot-dashed, dashed and solid lines refer respectively to $M_\nu = 0, 0.16, 0.32$ eV.

the peculiar velocity field. Moreover, as already pointed out, we can also observe how the increase in M_ν seems to impact the kinematic SZ less than the thermal one. We now study in detail the pixel distribution of this kSZ $\Delta T/T$ signal in the lower resolution (0.5°) maps, from which we remove the null pixels, as for the previous case. We find the best-fit with a Cauchy distribution

$$P(x) = \frac{1}{\pi C} \frac{1}{1 + \left(\frac{x-\mu}{C}\right)^2} \quad (5.1)$$

with mean μ and scale parameter C . The fitting values for the two parameters are listed in Table 5: as expected, the mean is in all simulations comparable to zero as it is at least one order of magnitude smaller with respect to C . When increasing neutrino mass, at fixed dark energy EoS, the scale parameter decreases leading to a more peaked distribution. Again it is possible to see the effect of incrementing the mass budget for neutrinos: due to the reduced number of haloes in the high-mass end the values closer to zero are favoured, as they derive from smaller structures with an accordingly smaller optical depth. Examples of the distributions are shown in Figure 10. Our finding differs substantially from those of [20, 42], obtained through hydrodynamical simulations, where the resulting distribution is a Gaussian curve rather than a Cauchy one. This confirms how our cluster-only analysis gives a partial picture of kSZ, missing an important part of signal with lower intensity, arising in diffuse gas.

Simulation		$10^8 \mu$	$10^8 C$
$M_\nu = 0 \text{ eV}$	$w_0 = -1, w_a = 0$	0.22	10.41
	$w_0 = -0.9, w_a = -0.3$	0.24	10.77
	$w_0 = -0.9, w_a = +0.3$	0.02	8.94
	$w_0 = -1.1, w_a = -0.3$	0.28	11.36
	$w_0 = -1.1, w_a = +0.3$	0.20	10.33
$M_\nu = 0.16 \text{ eV}$	$w_0 = -1, w_a = 0$	0.11	9.20
	$w_0 = -0.9, w_a = -0.3$	0.05	9.31
	$w_0 = -0.9, w_a = +0.3$	-0.07	7.33
	$w_0 = -1.1, w_a = -0.3$	0.12	9.70
	$w_0 = -1.1, w_a = +0.3$	0.04	8.87
$M_\nu = 0.32 \text{ eV}$	$w_0 = -1, w_a = 0$	-0.08	7.34
	$w_0 = -0.9, w_a = -0.3$	-0.01	7.22
	$w_0 = -0.9, w_a = +0.3$	-0.11	5.72
	$w_0 = -1.1, w_a = -0.3$	-0.02	7.90
	$w_0 = -1.1, w_a = +0.3$	-0.07	7.06

Table 5: Best-fit parameters C and μ for the Cauchy distribution of Equation (5.1), for all the DEMNUni simulations.

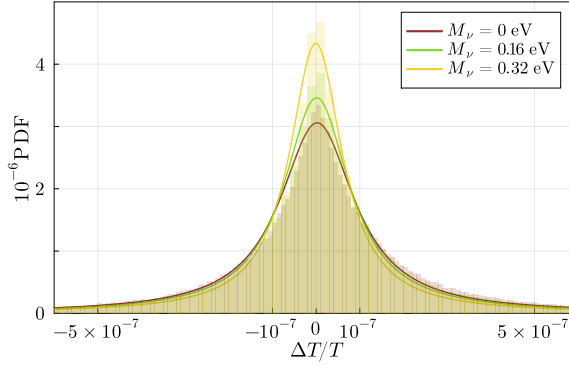


Figure 10: Best-fit Cauchy distribution for the kSZ $\Delta T/T$, compared to its normalised distribution in the sky for the cosmological constant simulations (number 1, 2 and 3 in Table 1).

5.2 Power spectrum

We compute the power spectrum of the cluster component of the kinematic SZ effect in the same way as for the tSZ, and obtain the results shown in Figure 11. Due to the partial description that our model provides the kSZ lacks power if compared to a more precise modelling (again see e.g. [20, 42]), especially at small scales. Nonetheless, a similar behaviour to that of the thermal effect can be observed, where both a different dark energy EoS and a different M_ν have a significant, and almost degenerate, impact on the power spectrum. With respect to the tSZ, for the kSZ we observe a less prominent dependence on the mass of the neutrino component: this is due to the increased contribution to the total power from the smaller haloes, the presence of which is less influenced by a change in M_ν . Also, at fixed M_ν , there is less tendency to converge at the smallest scales with respect to the tSZ, as for $\ell = 100$

the range in power covered by the possible EoS is greater than at $\ell = 10^4$ by 44, 43 and 39% for the $M_\nu = 0, 0.16$ and 0.32 eV models, respectively. The differences in the two effects become even more clear when explicitly looking at the ratio kSZ/tSZ, shown in Figure 12, where a growth both towards smaller scales and larger scales is present, respectively for $\ell \gtrsim 3000$ and $\ell \lesssim 300$. The latter is due to the peculiar velocity field, which has significant variability on very large scales (up to 400 Mpc) as it is mainly driven by linear, large scale evolution, while the density field varies on scales which are smaller.

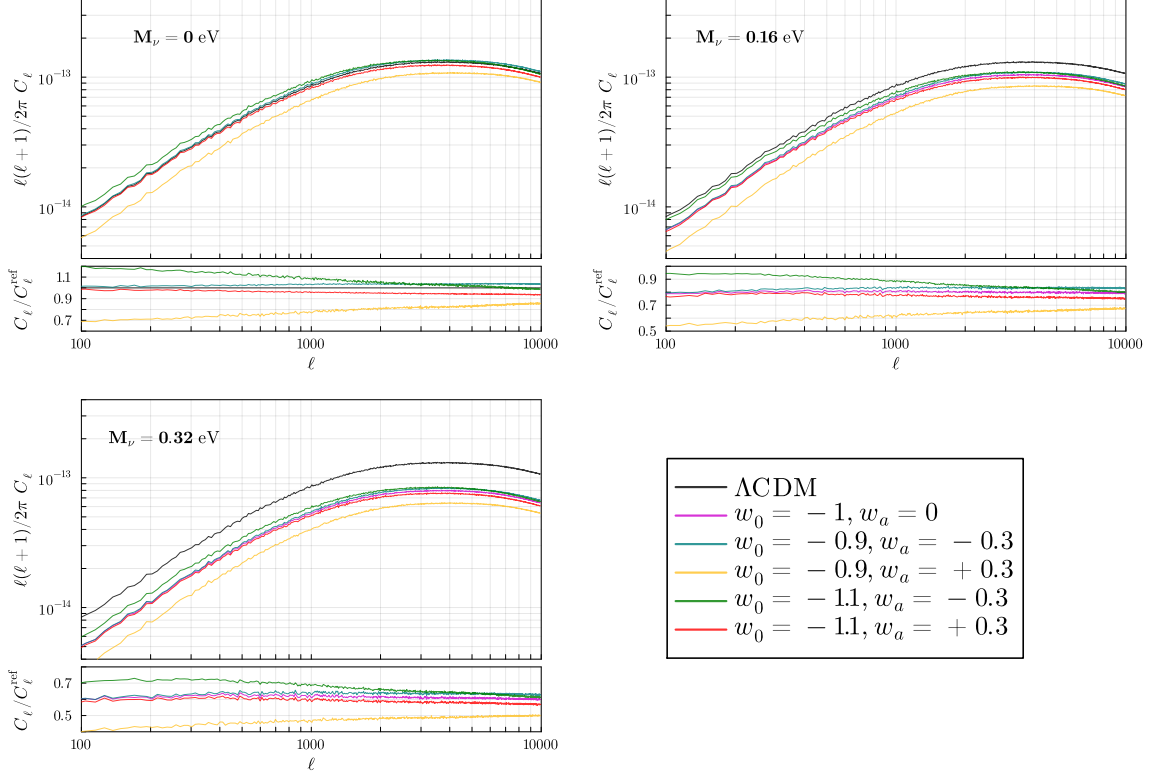


Figure 11: Power spectra of the kSZ effect for the 15 DEMNUni simulations, for $z > 0.05$. Top-left are massless simulations, top-right is $M_\nu = 0.16$ eV and bottom is $M_\nu = 0.32$ eV. Notice how in our cluster-only model the shape is similar to that of the thermal effect (see Figure 6). The panels also show the ratio of the different spectra with respect to the Λ CDM simulation.

We then study the dependence of the power spectrum on σ_8^{cb} also for the case of the kSZ. In the literature there are reported values for the scaling with different parameters [68], but always referred to the total kinematic effect, where diffuse matter is also present. Assuming that it is possible to neglect the small variations in Ω_{cb} , like we did for the tSZ, we fit the power-law scaling of the power spectrum as in Eq. (4.6), and find the results listed in Table 6. As expected, the dependencies are weaker with respect to those of the thermal effect in our investigation, as the number of smaller haloes is less affected by σ_8^{cb} . Conversely, these values are larger than the ones from the literature regarding the total kSZ, as the lack of a diffuse component in our analysis makes the kinematic power spectrum more sensitive to clustering.

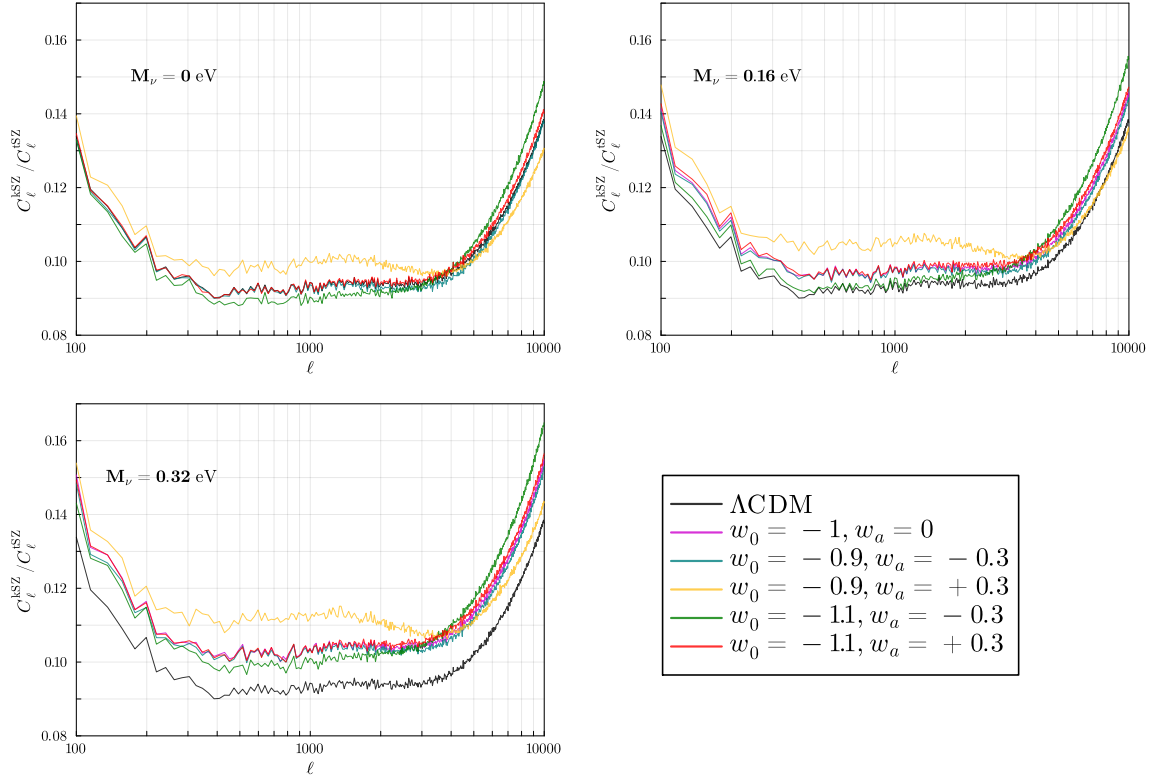


Figure 12: Ratio of the power spectra $C_\ell^{\text{kSZ}}/C_\ell^{\text{tSZ}}$ for the DEMNUni set, in the case of a frequency of 280 GHz, for which $g(x) = 1$. Top-left is $M_\nu = 0$ eV, top-right is $M_\nu = 0.16$ eV and bottom is $M_\nu = 0.32$ eV. The ratio slightly grows for more massive neutrinos, coherently with the reduced dependence of the kinematic effect on larger clusters.

(w_0, w_a)	q
$(-1, 0)$	6.1
$(-0.9, -0.3)$	6.2
$(-0.9, +0.3)$	6.5
$(-1.1, -0.3)$	5.9
$(-1.1, +0.3)$	6.1

Table 6: Power-law exponent for the scaling of the kSZ effect power spectrum with respect to σ_8^{cb} only. The calculation is analogous to the one for the tSZ, i.e. done keeping a fixed dark energy EoS and varying M_ν .

6 Conclusions

In this work we studied how extensions of the standard Λ CDM cosmology, namely massive neutrinos and a dynamical dark energy, affect the properties of the SZ effect of the large-scale structure of the Universe. We used the 15 DEMNUni cosmological N -body simulations [9, 10], that describe the evolution of the cosmic structures assuming different neutrino masses and dark energy EoS (summarized in Table 1) and built up a model to describe the properties of the baryonic component, modelling the SZ signal arising from galaxy clusters/groups via

scaling relations.

Starting from the simulation outputs, we identified the haloes via the **FoF** and **Subfind** algorithms, and built up mock lightcones using their outputs. We then used the prescription by [43] to model the pressure profile for each halo with $M_{200} > 3.4 \times 10^{13} h^{-1} M_{\odot}$ and construct a set of full-sky maps of the Compton- y parameter, and analysed the properties of the thermal SZ effect based on those. Our main results can be summarised as follows.

- We observe that the mean logarithmic Compton- y parameter reduces approximately as $10f_{\nu}$, regardless of the EoS of dark energy. This is analogous to the nonlinear damping caused by massive neutrinos in the matter power spectrum [69].
- The distribution of the Compton- y in logarithmic scale is, for all simulations, well described by a skewed Gaussian. At fixed dark energy EoS, an increase in M_{ν} translates into an increase of both the skewness and the variance of the curve.
- The power spectra of the tSZ effect are characterised by a similar shape, regardless of the simulation, and with the haloes at $z < 0.5$ being the main source of power for $\ell \lesssim 1000$. The effects of adding M_{ν} and a variable dark energy are mainly degenerate, and consist of a simple rescaling of the power spectrum; differences can be seen only for $\ell \gtrsim 2000$.
- We observe that the tSZ power spectrum scales, at a fixed dark energy EoS, as a power-law with respect to the parameter σ_8^{cb} , with an exponent varying from 7.2 to 8.2. This strong dependence reflects the importance of the high-mass end of the HMF for sourcing the tSZ effect. Conversely, we find that σ_8^{cb} can not trace the variation of the power spectrum when varying the dark energy EoS at fixed M_{ν} .
- Models with massless neutrinos overestimate consistently Planck data at $\ell > 300$, even when assuming an EoS that slows down cluster formation ($\chi^2 = 1.97$).
- On the other hand, 4 models fit equally well the Planck data at $\ell > 300$: one with $M_{\nu} = 0.16$ and $(w_0, w_a) = (-0.9, +0.3)$ and three with $M_{\nu} = 0.32$ eV and $(w_0, w_a) = (-1, 0), (-0.9, -0.3), (-1.1, +0.3)$. Their power spectra are highly degenerate for $\ell \lesssim 2000$.
- We produce cumulative SNR forecasts for observations of the tSZ effect with the Simons Observatory LAT instrument, based on its most realistic noise model, with values ranging from $\text{SNR} = 15$ ($M_{\nu} = 0.32$ eV with $(w_0, w_a) = (-0.9, +0.3)$) to $\text{SNR} = 27$ ($M_{\nu} = 0$ with $(w_0, w_a) = (-0.9, -0.3)$). Also, we derive estimates on the detectability of differences from the reference massless neutrino ΛCDM cosmology with a signal-to-noise χ^2 ; these show that most likely SO will be able to discriminate between ΛCDM and cosmologies with $M_{\nu} = 0.32$ eV, as well as most of those with $M_{\nu} = 0.16$ eV (aside from the $(w_0, w_a) = (-0.9, -0.3)$ one), but not between different dark energy EoS in the $M_{\nu} = 0$ scenario.

Regarding the kSZ effect, our description of the baryonic component is limited to galaxy clusters and groups and lacks the diffuse component that is expected to dominate the signal. With this caveat, by assigning each halo an NFW matter density profile we created and studied temperature maps, finding the following.

- The kinematic $\Delta T/T$ signal can be described by a Cauchy distribution, with a mean comparable to zero and a scale which reduces when increasing M_ν .
- The kSZ power spectrum in our model is around one order of magnitude smaller than its thermal counterpart (at 280 GHz), but exhibits a similar shape.
- The power of the kSZ effect also exhibits a similar behaviour to that of the thermal effect, with respect to a variable dark energy EoS and different M_ν values; yet the dependence on the latter is less marked.
- Under the assumption that the cosmological parameters dependence of the kSZ power spectrum, in our model, can be treated as for the tSZ, we found that it scales, at a fixed EoS for dark energy, with σ_8^{cb} to the power of 5.9–6.5. This confirms how the kinematic effect has an important source also from smaller structures, which are less impacted by M_ν and therefore σ_8^{cb} .

Our work has shown how the Sunyaev-Zel'dovich effect, particularly with its thermal contribution, could be a powerful probe of cosmological models beyond the standard Λ CDM, due to its strong dependence on matter clustering and the amount of virialised structures. On the one hand the impact of a non-zero neutrino mass is particularly significant and will most likely be detected by future surveys. On the other hand, the equations of state for a dynamical dark energy considered in the DEMNUni set might not lead to detectable differences yet, especially for those leading to power spectra very close to the cosmological constant. Further investigations will be needed to gain more precise insights on the SZ effect, in particular combining the data from the upcoming CMB surveys with tailored hydrodynamical simulations, taking into account both massive neutrinos and a dynamical dark energy.

Acknowledgments

GF is supported by the STFC Ernest Rutherford fellowship.

References

- [1] D.N. Spergel, L. Verde, H.V. Peiris, E. Komatsu, M.R. Nolte, C.L. Bennett et al., *First-Year Wilkinson Microwave Anisotropy Probe (WMAP) Observations: Determination of Cosmological Parameters*, *The Astrophysical Journal Supplement Series* **148** (2003) 175 [[astro-ph/0302209](#)].
- [2] E. Komatsu, K.M. Smith, J. Dunkley, C.L. Bennett, B. Gold, G. Hinshaw et al., *Seven-year Wilkinson Microwave Anisotropy Probe (WMAP) Observations: Cosmological Interpretation*, *The Astrophysical Journal Supplement* **192** (2011) 18 [[1001.4538](#)].
- [3] Planck Collaboration, P.A.R. Ade, N. Aghanim, C. Armitage-Caplan, M. Arnaud, M. Ashdown et al., *Planck 2013 results. XVI. Cosmological parameters*, *Astronomy & Astrophysics* **571** (2014) A16 [[1303.5076](#)].
- [4] Planck Collaboration, P.A.R. Ade, N. Aghanim, M. Arnaud, M. Ashdown, J. Aumont et al., *Planck 2015 results. XIII. Cosmological parameters*, *Astronomy & Astrophysics* **594** (2016) A13 [[1502.01589](#)].
- [5] Planck Collaboration, N. Aghanim, Y. Akrami, M. Ashdown, J. Aumont, C. Baccigalupi et al., *Planck 2018 results. VI. Cosmological parameters*, *Astronomy & Astrophysics* **641** (2020) A6 [[1807.06209](#)].

- [6] T. Louis, A. La Posta, Z. Atkins, H.T. Jense, I. Abril-Cabezas, G.E. Addison et al., *The Atacama Cosmology Telescope: DR6 Power Spectra, Likelihoods and Λ CDM Parameters*, *arXiv e-prints* (2025) arXiv:2503.14452 [[2503.14452](#)].
- [7] E. Calabrese, J.C. Hill, H.T. Jense, A. La Posta, I. Abril-Cabezas, G.E. Addison et al., *The Atacama Cosmology Telescope: DR6 Constraints on Extended Cosmological Models*, *arXiv e-prints* (2025) arXiv:2503.14454 [[2503.14454](#)].
- [8] A.G. Adame, J. Aguilar, S. Ahlen, S. Alam, D.M. Alexander, M. Alvarez et al., *DESI 2024 VI: cosmological constraints from the measurements of baryon acoustic oscillations*, *Journal of Cosmology and Astroparticle Physics* **2025** (2025) 021 [[2404.03002](#)].
- [9] C. Carbone, M. Petkova and K. Dolag, *DEMNUi: ISW, Rees-Sciama, and weak-lensing in the presence of massive neutrinos*, *Journal of Cosmology and Astroparticle Physics* **2016** (2016) 034 [[1605.02024](#)].
- [10] G. Parimbelli, C. Carbone, J. Bel, B. Bose, M. Calabrese, E. Carella et al., *DEMNUi: comparing nonlinear power spectra prescriptions in the presence of massive neutrinos and dynamical dark energy*, *Journal of Cosmology and Astroparticle Physics* **2022** (2022) 041 [[2207.13677](#)].
- [11] R. Kugel, J. Schaye, M. Schaller, I.G. McCarthy, J. Braspenning, J.C. Helly et al., *The FLAMINGO project: a comparison of galaxy cluster samples selected on mass, X-ray luminosity, Compton-Y parameter, or galaxy richness*, *Monthly Notices of the Royal Astronomical Society* **534** (2024) 2378 [[2406.03180](#)].
- [12] A. La Posta, D. Alonso, N.E. Chisari, T. Ferreira and C. García-García, *X + y: insights on gas thermodynamics from the combination of X-ray and thermal Sunyaev-Zel'dovich data cross-correlated with cosmic shear*, *arXiv e-prints* (2024) arXiv:2412.12081 [[2412.12081](#)].
- [13] L. Bigwood, A. Amon, A. Schneider, J. Salcido, I.G. McCarthy, C. Preston et al., *Weak lensing combined with the kinetic Sunyaev-Zel'dovich effect: a study of baryonic feedback*, *Monthly Notices of the Royal Astronomical Society* **534** (2024) 655 [[2404.06098](#)].
- [14] R.H. Liu, S. Ferraro, E. Schaan, R. Zhou, J.N. Aguilar, S. Ahlen et al., *Measurements of the Thermal Sunyaev-Zel'dovich Effect with ACT and DESI Luminous Red Galaxies*, *arXiv e-prints* (2025) arXiv:2502.08850 [[2502.08850](#)].
- [15] E. Schiappucci, S. Raghunathan, C. To, F. Bianchini, C.L. Reichardt, N. Battaglia et al., *Constraining cosmological parameters using the pairwise kinematic Sunyaev-Zel'dovich effect with CMB-S4 and future galaxy cluster surveys*, *arXiv e-prints* (2024) arXiv:2409.18368 [[2409.18368](#)].
- [16] B. Soergel, A. Saro, T. Giannantonio, G. Efstathiou and K. Dolag, *Cosmology with the pairwise kinematic SZ effect: calibration and validation using hydrodynamical simulations*, *Monthly Notices of the Royal Astronomical Society* **478** (2018) 5320 [[1712.05714](#)].
- [17] Y.-K. Chiang, R. Makiya, B. Ménard and E. Komatsu, *The Cosmic Thermal History Probed by Sunyaev-Zeldovich Effect Tomography*, *The Astrophysical Journal* **902** (2020) 56 [[2006.14650](#)].
- [18] Y. Fukuda, T. Hayakawa, E. Ichihara, K. Inoue, K. Ishihara, H. Ishino et al., *Evidence for Oscillation of Atmospheric Neutrinos*, *Physical Review Letters* **81** (1998) 1562 [[hep-ex/9807003](#)].
- [19] M. Roncarelli, C. Carbone and L. Moscardini, *The effect of massive neutrinos on the Sunyaev-Zel'dovich and X-ray observables of galaxy clusters*, *Monthly Notices of the Royal Astronomical Society* **447** (2015) 1761 [[1409.4285](#)].
- [20] M. Roncarelli, F. Villaescusa-Navarro and M. Baldi, *The kinematic Sunyaev-Zel'dovich effect of the large-scale structure (I): dependence on neutrino mass*, *Monthly Notices of the Royal Astronomical Society* **467** (2017) 985 [[1702.00676](#)].

- [21] S. Alam, M. Ata, S. Bailey, F. Beutler, D. Bizyaev, J.A. Blazek et al., *The clustering of galaxies in the completed SDSS-III Baryon Oscillation Spectroscopic Survey: cosmological analysis of the DR12 galaxy sample*, *Monthly Notices of the Royal Astronomical Society* **470** (2017) 2617 [[1607.03155](#)].
- [22] T.M.C. Abbott, M. Agüena, A. Alarcon, O. Alves, A. Amon, F. Andrade-Oliveira et al., *Dark Energy Survey Year 3 results: Constraints on extensions to Λ CDM with weak lensing and galaxy clustering*, *Physical Review D* **107** (2023) 083504 [[2207.05766](#)].
- [23] A.J. Tishue, S.C. Hotinli, P. Adshead, E.D. Kovetz and M.S. Madhavacheril, *Neutrino Mass Constraints from kSZ Tomography*, *arXiv e-prints* (2025) [arXiv:2502.05260](#) [[2502.05260](#)].
- [24] J. Lesgourgues and S. Pastor, *Massive neutrinos and cosmology*, *Physics Reports* **429** (2006) 307 [[astro-ph/0603494](#)].
- [25] J. Lesgourgues, G. Mangano, G. Miele and S. Pastor, *Neutrino Cosmology*, Cambridge University Press (2013).
- [26] R.L. Workman, V.D. Burkert, V. Crede, E. Klempt, U. Thoma, L. Tiator et al., *Review of Particle Physics*, *Progress of Theoretical and Experimental Physics* **2022** (2022) 083C01.
- [27] M. Chevallier and D. Polarski, *Accelerating Universes with Scaling Dark Matter*, *International Journal of Modern Physics D* **10** (2001) 213 [[gr-qc/0009008](#)].
- [28] E.V. Linder, *Exploring the Expansion History of the Universe*, *Physical Review Letters* **90** (2003) 091301 [[astro-ph/0208512](#)].
- [29] V. Springel, *The cosmological simulation code gadget-2*, *Monthly Notices of the Royal Astronomical Society* **364** (2005) 1105–1134.
- [30] M. Viel, M.G. Haehnelt and V. Springel, *The effect of neutrinos on the matter distribution as probed by the intergalactic medium*, *Journal of Cosmology and Astroparticle Physics* **2010** (2010) 015–015.
- [31] V. Springel, S.D.M. White, G. Tormen and G. Kauffmann, *Populating a cluster of galaxies - I. Results at $[f\sigma_{\text{mu2}}]z=0$* , *Monthly Notices of the Royal Astronomical Society* **328** (2001) 726 [[astro-ph/0012055](#)].
- [32] K. Dolag, S. Borgani, G. Murante and V. Springel, *Substructures in hydrodynamical cluster simulations*, *Monthly Notices of the Royal Astronomical Society* **399** (2009) 497 [[0808.3401](#)].
- [33] C. Carbone, V. Springel, C. Baccigalupi, M. Bartelmann and S. Matarrese, *Full-sky maps for gravitational lensing of the cosmic microwave background*, *Monthly Notices of the Royal Astronomical Society* **388** (2008) 1618 [[0711.2655](#)].
- [34] M. Calabrese, C. Carbone, G. Fabbian, M. Baldi and C. Baccigalupi, *Multiple lensing of the cosmic microwave background anisotropies*, *Journal of Cosmology and Astroparticle Physics* **3** (2015) 049 [[1409.7680](#)].
- [35] G. Fabbian, M. Calabrese and C. Carbone, *CMB weak-lensing beyond the Born approximation: a numerical approach*, *Journal of Cosmology and Astroparticle Physics* **2018** (2018) 050 [[1702.03317](#)].
- [36] S. Hilbert, A. Barreira, G. Fabbian, P. Fosalba, C. Giocoli, S. Bose et al., *The accuracy of weak lensing simulations*, *Monthly Notices of the Royal Astronomical Society* **493** (2020) 305 [[1910.10625](#)].
- [37] Euclid Collaboration, Y. Mellier, Abdurro'uf, J.A. Acevedo Barroso, A. Achúcarro, J. Adamek et al., *Euclid. I. Overview of the Euclid mission*, *arXiv e-prints* (2024) [arXiv:2405.13491](#) [[2405.13491](#)].
- [38] A.S. Kompaneets, *The Establishment of Thermal Equilibrium between Quanta and Electrons*, *Soviet Journal of Experimental and Theoretical Physics* **4** (1957) 730.

- [39] Y.B. Zel’dovich and R.A. Sunyaev, *The Interaction of Matter and Radiation in a Hot-Model Universe*, *Astrophysics and Space Science* **4** (1969) 301.
- [40] R.A. Sunyaev and Y.B. Zel’dovich, *Small-Scale Fluctuations of Relic Radiation*, *Astrophysics and Space Science* **7** (1970) 3.
- [41] R.A. Sunyaev, *Fluctuations in microwave background radiation due to secondary ionization of the intergalactic gas in the universe.*, *Pisma v Astronomicheskii Zhurnal* **3** (1977) 491.
- [42] M. Roncarelli, M. Baldi and F. Villaescusa-Navarro, *The kinematic Sunyaev-Zel’dovich effect of the large-scale structure (II): the effect of modified gravity*, *Monthly Notices of the Royal Astronomical Society* **481** (2018) 2497 [[1805.11607](#)].
- [43] N. Battaglia, J.R. Bond, C. Pfrommer and J.L. Sievers, *On the Cluster Physics of Sunyaev-Zel’dovich and X-Ray Surveys. II. Deconstructing the Thermal SZ Power Spectrum*, *The Astrophysical Journal* **758** (2012) 75 [[1109.3711](#)].
- [44] A. Cooray, D. Baumann and K. Sigurdson, *Statistical imprints of SZ effects in the cosmic microwave background*, in *Background Microwave Radiation and Intracluster Cosmology*, F. Melchiorri and Y. Rephaeli, eds., p. 309, Jan., 2005, DOI [[astro-ph/0410006](#)].
- [45] J.C. Hill and E. Pajer, *Cosmology from the thermal Sunyaev-Zel’dovich power spectrum: Primordial non-Gaussianity and massive neutrinos*, *Physical Review D* **88** (2013) 063526 [[1303.4726](#)].
- [46] J.F. Navarro, C.S. Frenk and S.D.M. White, *The Structure of Cold Dark Matter Halos*, *The Astrophysical Journal* **462** (1996) 563 [[astro-ph/9508025](#)].
- [47] A.R. Duffy, J. Schaye, S.T. Kay and C. Dalla Vecchia, *Dark matter halo concentrations in the Wilkinson Microwave Anisotropy Probe year 5 cosmology*, *Monthly Notices of the Royal Astronomical Society* **390** (2008) L64 [[0804.2486](#)].
- [48] M.R. Calabretta and E.W. Greisen, *Representations of celestial coordinates in FITS*, *Astronomy & Astrophysics* **395** (2002) 1077 [[astro-ph/0207413](#)].
- [49] A. Azzalini, *A class of distributions which includes the normal ones*, *Scandinavian Journal of Statistics* **12** (1985) 171.
- [50] B. Bolliet, A. Kusiak, F. McCarthy, A. Sabyr, K. Surrao, J.C. Hill et al., *class_sz I: Overview*, *arXiv e-prints* (2023) [arXiv:2310.18482](#) [[2310.18482](#)].
- [51] B. Bolliet, J. Colin Hill, S. Ferraro, A. Kusiak and A. Krolewski, *Projected-field kinetic Sunyaev-Zel’dovich Cross-correlations: halo model and forecasts*, *Journal of Cosmology and Astroparticle Physics* **2023** (2023) 039 [[2208.07847](#)].
- [52] J.L. Tinker, B.E. Robertson, A.V. Kravtsov, A. Klypin, M.S. Warren, G. Yepes et al., *The Large-scale Bias of Dark Matter Halos: Numerical Calibration and Model Tests*, *The Astrophysical Journal* **724** (2010) 878 [[1001.3162](#)].
- [53] B. Bolliet, B. Comis, E. Komatsu and J.F. Macías-Pérez, *Dark energy constraints from the thermal Sunyaev-Zeldovich power spectrum*, *Monthly Notices of the Royal Astronomical Society* **477** (2018) 4957 [[1712.00788](#)].
- [54] Planck Collaboration, N. Aghanim, M. Arnaud, M. Ashdown, J. Aumont, C. Baccigalupi et al., *Planck 2015 results. XXII. A map of the thermal Sunyaev-Zeldovich effect*, *Astronomy & Astrophysics* **594** (2016) A22 [[1502.01596](#)].
- [55] A. Lewis, A. Challinor and A. Lasenby, *Efficient Computation of Cosmic Microwave Background Anisotropies in Closed Friedmann-Robertson-Walker Models*, *The Astrophysical Journal* **538** (2000) 473 [[astro-ph/9911177](#)].
- [56] A. Lewis and A. Challinor, “CAMB: Code for Anisotropies in the Microwave Background.” Astrophysics Source Code Library, Feb, 2011.

- [57] E. Komatsu and U. Seljak, *The Sunyaev-Zel'dovich angular power spectrum as a probe of cosmological parameters*, *Monthly Notices of the Royal Astronomical Society* **336** (2002) 1256 [[astro-ph/0205468](#)].
- [58] L.D. Shaw, D. Nagai, S. Bhattacharya and E.T. Lau, *Impact of Cluster Physics on the Sunyaev-Zel'dovich Power Spectrum*, *The Astrophysical Journal* **725** (2010) 1452 [[1006.1945](#)].
- [59] H. Trac, P. Bode and J.P. Ostriker, *Templates for the Sunyaev-Zel'dovich Angular Power Spectrum*, *The Astrophysical Journal* **727** (2011) 94 [[1006.2828](#)].
- [60] B. Bolliet, T. Brinckmann, J. Chluba and J. Lesgourgues, *Including massive neutrinos in thermal Sunyaev Zeldovich power spectrum and cluster counts analyses*, *Monthly Notices of the Royal Astronomical Society* **497** (2020) 1332 [[1906.10359](#)].
- [61] E. Castorina, E. Sefusatti, R.K. Sheth, F. Villaescusa-Navarro and M. Viel, *Cosmology with massive neutrinos II: on the universality of the halo mass function and bias*, *Journal of Cosmology and Astroparticle Physics* **2014** (2014) 049 [[1311.1212](#)].
- [62] M. LoVerde, *Spherical collapse in $\nu\Lambda$ CDM*, *Physical Review D* **90** (2014) 083518 [[1405.4858](#)].
- [63] J. Tinker, A.V. Kravtsov, A. Klypin, K. Abazajian, M. Warren, G. Yepes et al., *Toward a Halo Mass Function for Precision Cosmology: The Limits of Universality*, *The Astrophysical Journal* **688** (2008) 709 [[0803.2706](#)].
- [64] P. Ade, J. Aguirre, Z. Ahmed, S. Aiola, A. Ali, D. Alonso et al., *The Simons Observatory: science goals and forecasts*, *Journal of Cosmology and Astroparticle Physics* **2019** (2019) 056 [[1808.07445](#)].
- [65] P. Singh, B.B. Nath, S. Majumdar and J. Silk, *CMB distortion from circumgalactic gas*, *Monthly Notices of the Royal Astronomical Society* **448** (2015) 2384 [[1408.4896](#)].
- [66] R. Makiya, S. Ando and E. Komatsu, *Joint analysis of the thermal Sunyaev-Zeldovich effect and 2MASS galaxies: probing gas physics in the local Universe and beyond*, *Monthly Notices of the Royal Astronomical Society* **480** (2018) 3928 [[1804.05008](#)].
- [67] A.R. Pullen, S. Alam and S. Ho, *Probing gravity at large scales through CMB lensing*, *Monthly Notices of the Royal Astronomical Society* **449** (2015) 4326 [[1412.4454](#)].
- [68] L.D. Shaw, D.H. Rudd and D. Nagai, *Deconstructing the Kinetic SZ Power Spectrum*, *The Astrophysical Journal* **756** (2012) 15 [[1109.0553](#)].
- [69] S. Bird, M. Viel and M.G. Haehnelt, *Massive neutrinos and the non-linear matter power spectrum*, *Monthly Notices of the Royal Astronomical Society* **420** (2012) 2551 [[1109.4416](#)].